LETTER

doi:10.1038/nature20169

The SND proteins constitute an alternative targeting route to the endoplasmic reticulum

Naama Aviram[1], Tslil Ast[1]†, Elizabeth A. Costa[2], Eric C. Arakel[3], Silvia G. Chuartzman[1], Calvin H. Jan[2], Sarah Haßdenteufel[4], Johanna Dudek[4], Martin Jung[4], Stefan Schorr[4], Richard Zimmermann[4], Blanche Schwappach[3,5], Jonathan S. Weissman[2] & Maya Schuldiner[1]

In eukaryotes, up to one-third of cellular proteins are targeted to the endoplasmic reticulum, where they undergo folding, processing, sorting and trafficking to subsequent endomembrane compartments[1]. Targeting to the endoplasmic reticulum has been shown to occur co-translationally by the signal recognition particle (SRP) pathway[2] or post-translationally by the mammalian transmembrane recognition complex of 40 kDa (TRC40)[3,4] and homologous yeast guided entry of tail-anchored proteins (GET)[5,6] pathways. Despite the range of proteins that can be catered for by these two pathways, many proteins are still known to be independent of both SRP and GET, so there seems to be a critical need for an additional dedicated pathway for endoplasmic reticulum relay[7,8]. We set out to uncover additional targeting proteins using unbiased high-content screening approaches. To this end, we performed a systematic visual screen using the yeast *Saccharomyces cerevisiae*[9,10], and uncovered three uncharacterized proteins whose loss affected targeting. We suggest that these proteins work together and demonstrate that they function in parallel with SRP and GET to target a broad range of substrates to the endoplasmic reticulum. The three proteins, which we name Snd1, Snd2 and Snd3 (for SRP-independent targeting), can synthetically compensate for the loss of both the SRP and GET pathways, and act as a backup targeting system. This explains why it has previously been difficult to demonstrate complete loss of targeting for some substrates. Our discovery thus puts in place an essential piece of the endoplasmic reticulum targeting puzzle, highlighting how the targeting apparatus of the eukaryotic cell is robust, interlinked and flexible.

To uncover factors that contribute to endoplasmic reticulum (ER) targeting, we devised a high-content screen in the yeast *S. cerevisiae* (Fig. 1a). We followed the fate of a model substrate, Gas1, which is known to be completely SRP-independent and only partially dependent on GET for targeting to the ER[9,10]. Using automated techniques[11,12], we integrated fluorescently tagged Gas1 (RFP–Gas1) into around 6,000 strains harbouring mutations in every yeast gene[13,14] and imaged them on an automated fluorescence microscopy platform[15]. We visually searched for strains in which Gas1 localized differently from wild-type or negative controls (where it localizes to the cell walls and vacuoles; Fig. 1b, Extended Data Fig. 1a). In strains mutated in the canonical translocon subunit Sec61 (ref. 16), the auxiliary complex that facilitates SRP-independent translocation (Sec62, Sec63, Sec66, Sec72)[17] or the GET pathway (Get3)[6], Gas1 accumulated in the cytosol, where it aggregated as expected (Fig. 1b) (for a full list of genes that displayed an altered phenotype, see Supplementary Table 1).

Three uncharacterized mutants showed a similar mislocalization effect to the Δ*get3* strain (Fig. 1b). Because the Gas1 foci that formed in the three mutants co-localized with a soluble misfolded marker[18] (Extended Data Fig. 1b), and as the mutants did not affect the localization of an SRP-dependent substrate (Extended Data Fig. 1c), we named these new elements SND (SRP-independent targeting) proteins.

Snd1 (encoded by *YDR186C*, here called *SND1*) is predicted to be soluble (Extended Data Fig. 1d), localizes to the cytosol[19] (Fig. 1c; for verification that all tagged SND proteins are functional see Extended Data Fig. 1e) and was proposed to be a peripheral ribosomal protein[20]. Snd2 (encoded by *ENV10*, also known as *YLR065C*, here called *SND2*) is predicted to have four transmembrane domains (Extended Data Fig. 1d), localizes to the ER membrane (Fig. 1c) and was previously shown to affect carboxypeptidase Y (CPY) maturation[21]. The human orthologue of Snd2, TMEM208 (here referred to as hSnd2), was previously shown to localize to the ER when tagged[22]. We confirmed localization of the native protein by raising antibodies against hSnd2 and could detect it in canine pancreatic microsomes and enriched in ER fractions of HEK293 cells (Extended Data Fig. 1f, g). The third protein, Snd3 (encoded by *PHO88*, also known as *YBR106W*, here called *SND3*), is predicted to have one transmembrane domain (Extended Data Fig. 1d), and is localized to the ER[19] (Fig. 1c). Loss of *SND3* has been shown to affect secretion of the yeast acid phosphatase via an unknown mechanism[23].

To investigate whether the SND proteins work cooperatively in a pathway or complex, we immunoprecipitated GFP–Snd2 and Snd3–GFP. Mass spectrometry analysis showed that both of them interacted physically with components of the targeting and translocation apparatus of the cell (Supplementary Table 2). Interestingly, GFP–Snd2 pull-downs were enriched for Snd1 (Supplementary Table 2). Snd2 also co-immunoprecipitated with Snd3 and Sec61 (Fig. 1d). Moreover, we found Snd2 and Snd3 in a complex with the translocon when assayed by blue native gel electrophoresis followed by SDS–PAGE (Extended Data Fig. 2a). In support of the idea that these proteins have a role in targeting substrates to the translocation machinery, we also detected an interaction between the Snd2–Snd3 complex and the cytosolic (that is, non translocated and unglycosylated) fraction of our model substrate, RFP–Gas1 (Fig. 1d).

Next, we found that the stability of Snd1 protein was compromised in the *SND2/SND3* double mutant (Fig. 1e). Conversely, localization of Snd2 and Snd3 was altered upon loss of other SND components (Extended Data Fig. 2b). We observed a synthetic sick interaction between Δ*snd3* and Δ*snd1* or Δ*snd2* when inspecting colony sizes (Extended Data Fig. 2c), but complete epistasis of Δ*snd3* with both Δ*snd1* and Δ*snd2* in their effect on Gas1 aggregation (Extended Data Fig. 2d, e). As the single deletion of *SND3* led to impaired growth (Extended Data Fig. 2c), and as the Snd3 protein is an order of magnitude more abundant than Snd1 or Snd2 (ref. 24), it is possible that its synthetic growth interaction results from an additional cellular role, unrelated to its common function with *SND1* and *SND2*. Together, these findings support the idea that the SND proteins function in a joint targeting pathway.

[1]Department of Molecular Genetics, Weizmann Institute of Science, Rehovot 7610001, Israel. [2]Department of Cellular and Molecular Pharmacology, UCSF California Institute for Quantitative Biomedical Research and Howard Hughes Medical Institute, San Francisco, California 94158-2330, USA. [3]Department of Molecular Biology, University Medical Center Göttingen, 37073 Göttingen, Germany. [4]Department of Medical Biochemistry and Molecular Biology, Saarland University, 66421 Homburg, Germany. [5]Max-Planck Institute for Biophysical Chemistry, 37077 Göttingen, Germany. †Present address: Broad Institute of Massachusetts Institute of Technology and Harvard, Cambridge, Massachusetts 02114, USA.

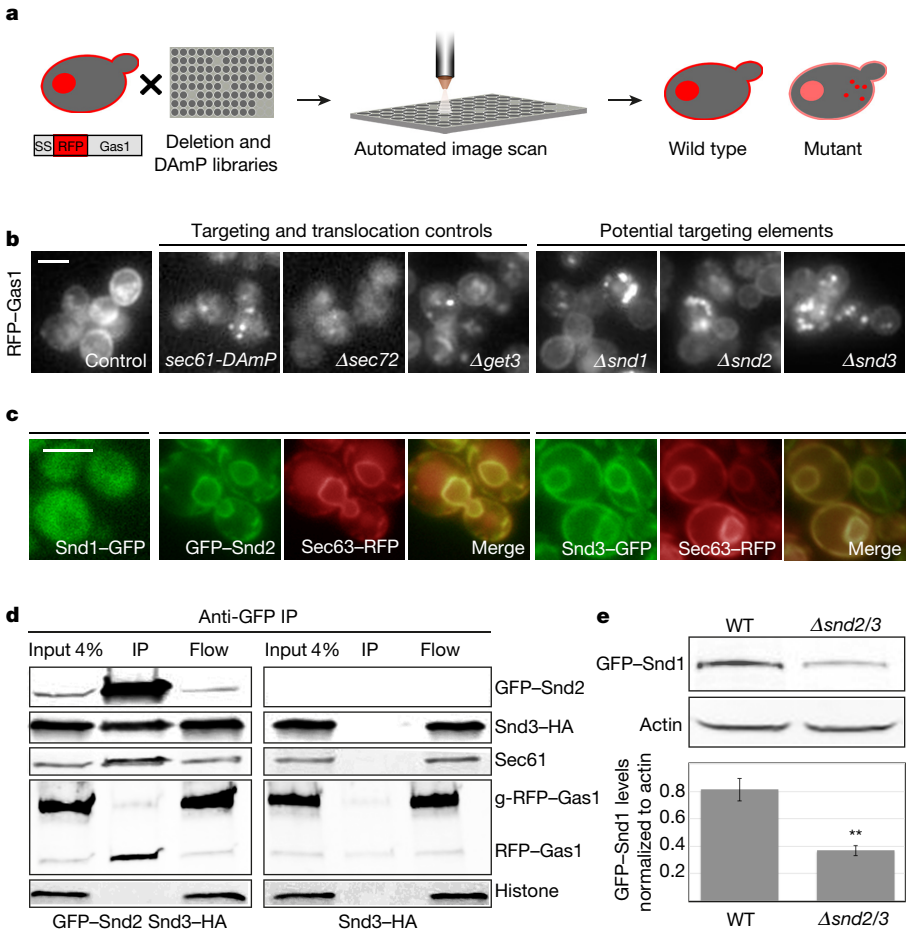

Figure 1 | A systematic screen uncovers uncharacterized ER targeting elements. a, A systematic screen for localization of SS-RFP–Gas1 on the background of yeast mutant libraries. SS, signal sequence. **b**, Mutants of *SND1*, *SND2* or *SND3* affect SS-RFP–Gas1 targeting similarly to known translocation or targeting mutants. **c**, Localization of GFP-tagged Snd1, Snd2 and Snd3. ER is marked by Sec63–RFP. **d**, Anti-GFP immunoprecipitation from GFP–Snd2/Snd3–HA strain and the negative control Snd3–HA strain. GFP–Snd2 co-immunoprecipitated with Snd3–HA, Sec61 and the uninserted, cytosolic form of RFP–Gas1. **e**, GFP–Snd1 levels are lower in the *Δsnd2/Δsnd3* double mutant compared to the wild type (WT). Data shown are means ± s.e.m. $^{**}P < 0.01$ by two-tailed Student's *t*-test, $n = 3$, biological replicates. For gel source images, see Supplementary Fig. 1. Scale bars, 5 μm. All images are representative of around 300 cells per strain.

To directly test whether SND proteins affect targeting and uncover their substrate range, we turned to proximity-specific ribosome profiling[25] (Fig. 2a). A subset of transcripts was depleted on the ER membrane in cells from all three *Δsnd* strains, providing independent evidence that the SND machinery has a role in targeting these substrates to the ER surface as they are being translated (Fig. 2b). The proteins most affected in the *snd* mutants have been previously shown to accumulate on the ER membrane in the presence of the translational inhibitor cycloheximide, indicative of targeting that is only loosely coupled to translation[25]. Notably, transcripts encoding proteins bearing an N-terminal transmembrane domain (TMD) (that is, in the first 95 amino acids, within the optimal recognition window of SRP[26]) did not appear to be effected, whereas proteins with more downstream TMDs were depleted in all three *Δsnd* strains (Fig. 2c; for a full list of transcripts affected in *SND* mutants, see Supplementary Table 3).

To verify the results of the ribosome-profiling assay, we assayed a representative secretory protein, Ynl181w, whose TMD is in the central portion of the protein. Indeed, Ynl181w showed reduced targeting in the *Δsnd* strains by both microscopy and *in-vivo* translocation assays (Fig. 2d, e).

Our data suggest that the location of the first TMD within the protein is a major determinant of SND targeting and therefore merely altering the relative position of the first TMD in the protein should alter its pathway dependence. To test this idea, we re-engineered two secretory substrates to alter their TMD positions and tested their targeting dependence. As predicted, simply moving the TMDs of two different substrates could alter their dependence on the SRP, SND or GET pathways (Fig. 2f, g and Extended Data Fig. 3).

Together, our results suggest either that SND proteins specifically recognize substrates with central TMDs or that SNDs cater for a broad substrate range, but their loss is only visible for those substrates not efficiently targeted by SRP or GET. To differentiate between these two possibilities, we investigated the relationship between the SNDs and the SRP and GET pathways.

To explore the interaction between the SNDs and the SRP pathway we used the previously described *sec65-1* temperature-sensitive strain, which has reduced SRP function at the permissive temperature and complete loss of SRP at the restrictive one. On this background we expressed the SND genes under the inducible *GAL1* promoter (Galp), which leads to either full repression (in glucose) or overexpression (in galactose). Slightly reduced SRP activity led to synthetic lethality in strains lacking *SND2* or *SND3* (Fig. 3a), whereas overexpression of *SND2* or *SND3* could rescue complete loss of SRP function (Fig. 3b), although Sec65 and Snd levels remained unchanged (Extended Data Fig. 4a, b). The restoration of viability was due to marked rescue of the cells' targeting capabilities by SND proteins (Fig. 3c, d and Extended Data Fig. 4c). These findings suggest that the SND proteins provide an alternate targeting route for a broad range of substrates, including targets that, under normal physiological conditions, are likely to be efficiently captured by SRP.

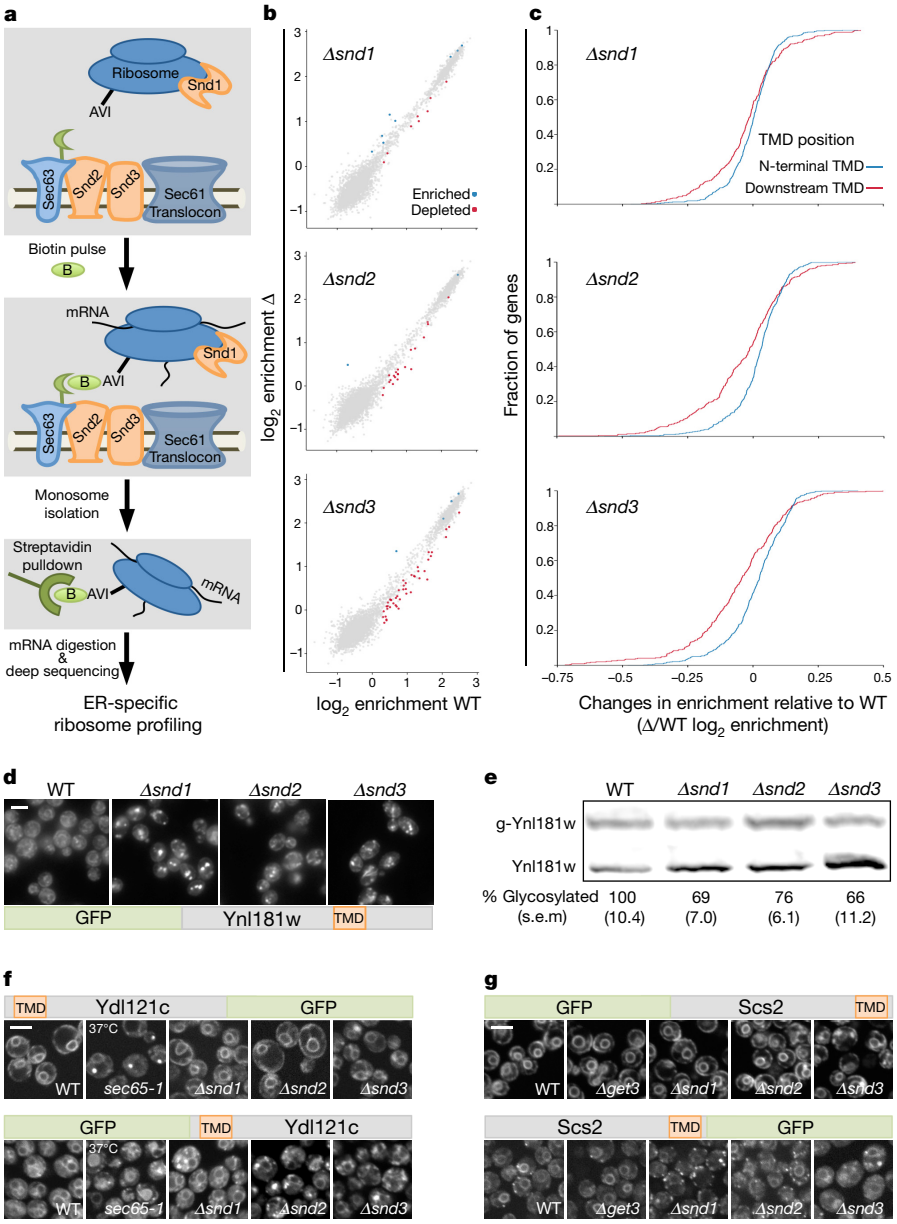

Figure 2 | SNDs affect the targeting of proteins with downstream transmembrane domains. a, Schematic of proximity-specific ribosome profiling. **b**, Translational enrichment on the ER surface. Significantly enriched or depleted transcripts in *Δsnd* mutants compared to wild type shown as blue or red circles, respectively. **c**, Cumulative distribution of ER enrichment of proteins with downstream TMDs (after 95 amino acids, red) or with an N-terminal TMD (in the first 95 amino acids, blue). **d**, Microscopy images of GFP–Ynl181w localization in *SND* mutants. **e**, Western blot of translocation efficiency of glycosylatable HA (HA-Gly)-tagged Ynl181w (data shown are means (s.e.m.), $n = 3$, biological replicates). g-Ynl181w, glycosylated. **f**, **g**, Microscopy images of localization of re-engineered Ydl121c (**f**) or Scs2 (**g**) on the background of targeting mutants. For gel source images, see Supplementary Fig. 1. Scale bars, 5 μm. All images are representative of around 300 cells per strain.

If SND proteins act as a targeting pathway with a broad substrate range, then the SND and GET pathways should also act as functional backups for each other. As previously shown[27], deletion of *SND* genes becomes lethal in the absence of members of the GET pathway (Fig. 4a). However, concomitant loss of *SND* genes in strains lacking the auxiliary translocon(*Δsec72*) has epistatic or additive effects, suggesting that the SNDs target proteins to the SRP-independent translocon (Extended Data Fig. 5a).

To ascertain that the cause of death of double *SND/GET* mutants lay in drastic alterations of targeting efficiency, we created a conditional double mutant for Snd2 and Get3, double deletion of which is synthetic lethal (Extended Data Fig. 5a, b). Metabolic labelling of RFP–Gas1 clearly demonstrated that although the single mutations (*Tetp-snd2* or *Δget3*) had only a small effect on translocation efficiency (Fig. 4b and Extended Data Fig. 5c, d), the double mutant showed a marked decrease in mature RFP–Gas1 (Fig. 4b). The same is true for the known GET pathway substrate, the tail-anchored protein Ysy6 (ref. 6) (Fig. 4c), verifying our hypothesis that the two pathways work in parallel to ensure robust targeting. Conversely, when we used this system to test CPY or the SRP-dependent substrate DHCαF, their translocation was not hampered in either the single or the double mutants (Fig. 4d and Extended Data Fig. 5e–g), excluding any secondary effects of the double knockdown.

Supporting our hypothesis that SND and GET have functional redundancy for targeting proteins with downstream targeting signals, we find that a synthetic construct of GFP fused to the C-terminal glycosylphosphatidylinositol (GPI)-anchoring sequence of Gas1 (GFP–AS_{Gas1})[9] can target well in the absence of either SND or GET but not in the

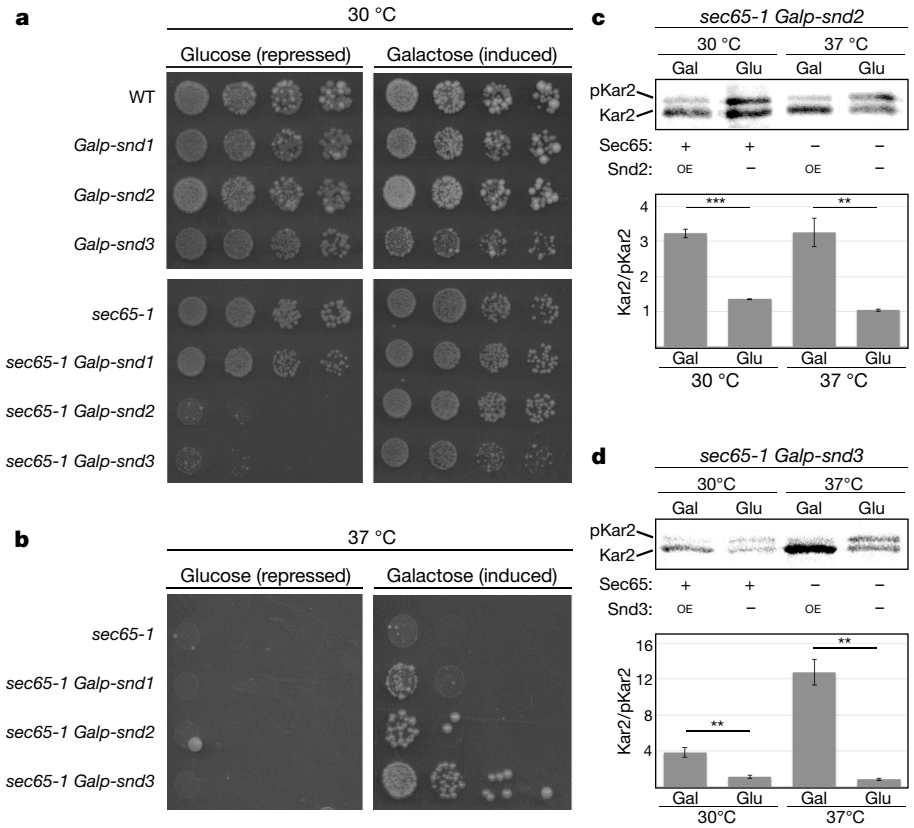

Figure 3 | SND proteins can compensate for loss of SRP. *SND* genes were expressed under the repressible (glucose) or inducible (galactose) Gal1 promoter. **a**, Growth at permissive temperature (30 °C, induces mild reduction in SRP). Repression of *SND*s leads to a synthetic sick or lethal phenotype. **b**, Growth at restrictive temperature (37 °C). Overexpression of *SND*s rescues lethality. **c**, **d**, Metabolic labelling of Kar2. When either *SND2* (**c**) or *SND3* (**d**) was overexpressed, Kar2 was translocated significantly better than when *SND2* or *SND3* were repressed (data shown are means ± s.e.m., $^{**}P < 0.01$, $^{***}P < 0.001$ by two-tailed Student's *t*-test, $n = 3$, biological replicates). Stronger Snd3-dependent translocation may explain the stronger rescue of this strain (**b**). For gel source images, see Supplementary Fig. 1.

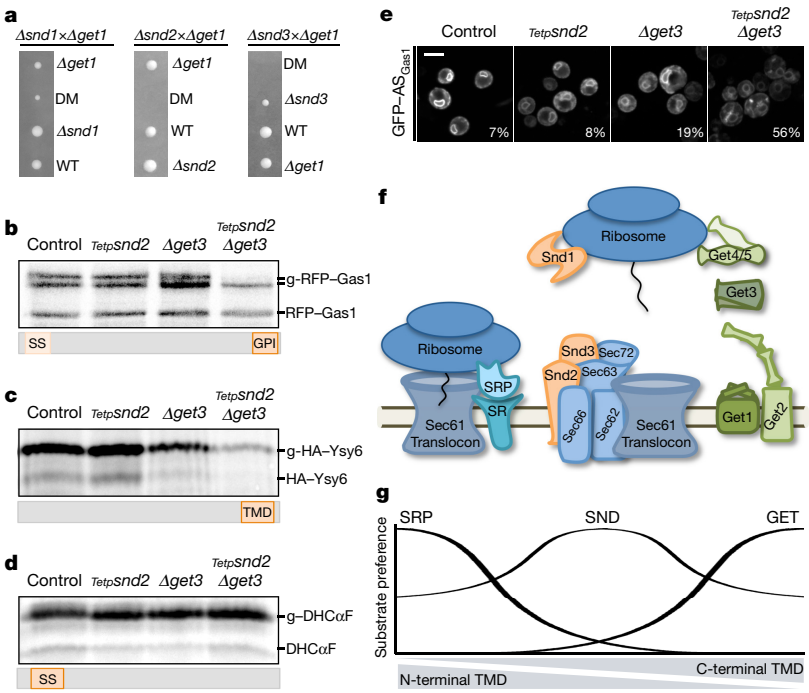

Figure 4 | The GET and SND pathways act as backups for targeting *in vivo*. **a**, Tetrads from *ΔsndΔget* diploids demonstrate a synthetic sick/lethal interaction. DM, double *ΔsndΔget* mutant. **b**–**d**, Metabolic labelling of RFP–Gas1 (**b**), HA–Ysy6 (**c**) and DHCαF (**d**) showing a decrease in translocated forms only for SRP-independent substrates in the conditional *SND2/GET3* double mutant. Accumulation of pre-inserted forms cannot be observed owing to lack of proteasomal inhibition. Results reproduced in three biological replicates. **e**, GFP fused to Gas1 GPI-anchoring sequence (GFP–AS$_{Gas1}$). Percentage of cells (from 100) with mistargeting depicted on images. Scale bar, 5 μm. **f**, Schematic of the eukaryotic ER-targeting apparatus. **g**, Model of the interplay among the ER-targeting pathways. For gel source images see Supplementary Fig. 1.

SND/GET double mutant (Fig. 4e). Hence, our results uncover the parallel functions of the SND and GET pathways in targeting proteins with downstream hydrophobic motifs.

Together, our data reveal that the SNDs can target diverse proteins with signals dispersed throughout the entire protein range. Moreover, they highlight a complex interconnected web with the two known targeting pathways that may explain the original difficulty in identifying the SND pathway.

Although its mechanistic details have yet to be uncovered, it is tempting to speculate about the mode of function of the SND pathway (Fig. 4f). As Snd1 is predicted to interact with ribosomes[20], it may be involved in capturing nascent substrates. Snd2 and Snd3, both ER transmembrane proteins that form a complex together with the translocon (Fig. 1d and Extended Data Fig. 2a), could act as receptors in promoting substrate capture and handoff to the translocon. It would be interesting to investigate whether the human orthologue hSnd2 has a similar role in mammalian cells.

Our data show that the three pathways, SRP, SND and GET, work in parallel to facilitate ER targeting of proteins bearing targeting motifs in all possible positions (Fig. 4g). If there is no distinct transmembrane position at which one pathway ceases to function and another steps in, but rather there exists a gradual decrease or increase in affinities, this would explain the substrate overlap between the pathways and the difficulties in reaching coherent understanding of the targeting requirements for many substrates[7]. More generally, identifying the role of the SND proteins demonstrates once again the intricacy and complexity of the cellular network engaged in efficient targeting.

Online Content Methods, along with any additional Extended Data display items and Source Data, are available in the online version of the paper; references unique to these sections appear only in the online paper.

Received 8 March; accepted 18 October 2016.

1. Rapoport, T. A. Protein translocation across the eukaryotic endoplasmic reticulum and bacterial plasma membranes. *Nature* **450,** 663–669 (2007).
2. Walter, P. & Johnson, A. E. Signal sequence recognition and protein targeting to the endoplasmic reticulum membrane. *Annu. Rev. Cell Biol.* **10,** 87–119 (1994).
3. Favaloro, V., Spasic, M., Schwappach, B. & Dobberstein, B. Distinct targeting pathways for the membrane insertion of tail-anchored (TA) proteins. *J. Cell Sci.* **121,** 1832–1840 (2008).
4. Stefanovic, S. & Hegde, R. S. Identification of a targeting factor for posttranslational membrane protein insertion into the ER. *Cell* **128,** 1147–1159 (2007).
5. Jonikas, M. C. *et al.* Comprehensive characterization of genes required for protein folding in the endoplasmic reticulum. *Science* **323,** 1693–1697 (2009).
6. Schuldiner, M. *et al.* The GET complex mediates insertion of tail-anchored proteins into the ER membrane. *Cell* **134,** 634–645 (2008).
7. Aviram, N. & Schuldiner, M. Embracing the void—how much do we really know about targeting and translocation to the endoplasmic reticulum? *Curr. Opin. Cell Biol.* **29,** 8–17 (2014).
8. Ast, T. & Schuldiner, M. All roads lead to Rome (but some may be harder to travel): SRP-independent translocation into the endoplasmic reticulum. *Crit. Rev. Biochem. Mol. Biol.* **48,** 273–288 (2013).
9. Ast, T., Cohen, G. & Schuldiner, M. A network of cytosolic factors targets SRP-independent proteins to the endoplasmic reticulum. *Cell* **152,** 1134–1145 (2013).
10. Ng, D. T., Brown, J. D. & Walter, P. Signal sequences specify the targeting route to the endoplasmic reticulum membrane. *J. Cell Biol.* **134,** 269–278 (1996).
11. Cohen, Y. & Schuldiner, M. Advanced methods for high-throughput microscopy screening of genetically modified yeast libraries. *Methods Mol. Biol.* **781,** 127–159 (2011).
12. Tong, A. H. Y. & Boone, C. Synthetic genetic array analysis in *Saccharomyces cerevisiae*. *Methods Mol. Biol.* **313,** 171–192 (2006).
13. Giaever, G. *et al.* Functional profiling of the *Saccharomyces cerevisiae* genome. *Nature* **418,** 387–391 (2002).
14. Breslow, D. K. *et al.* A comprehensive strategy enabling high-resolution functional analysis of the yeast genome. *Nat. Methods* **5,** 711–718 (2008).
15. Breker, M., Gymrek, M. & Schuldiner, M. A novel single-cell screening platform reveals proteome plasticity during yeast stress responses. *J. Cell Biol.* **200,** 839–850 (2013).
16. Mandon, E. C., Trueman, S. F. & Gilmore, R. Protein translocation across the rough endoplasmic reticulum. *Cold Spring Harb. Perspect. Biol.* **5,** 1–14 (2013).
17. Harada, Y., Li, H., Wall, J. S., Li, H. & Lennarz, W. J. Structural studies and the assembly of the heptameric post-translational translocon complex. *J. Biol. Chem.* **286,** 2956–2965 (2011).
18. Kaganovich, D., Kopito, R. & Frydman, J. Misfolded proteins partition between two distinct quality control compartments. *Nature* **454,** 1088–1095 (2008).
19. Huh, W.-K. *et al.* Global analysis of protein localization in budding yeast. *Nature* **425,** 686–691 (2003).
20. Fleischer, T. C., Weaver, C. M., McAfee, K. J., Jennings, J. L. & Link, A. J. Systematic identification and functional screens of uncharacterized proteins associated with eukaryotic ribosomal complexes. *Genes Dev.* **20,** 1294–1307 (2006).
21. Ricarte, F. *et al.* A genome-wide immunodetection screen in *S. cerevisiae* uncovers novel genes involved in lysosomal vacuole function and morphology. *PLoS One* **6,** e23696 (2011).
22. Zhao, Y. *et al.* Transmembrane protein 208: a novel ER-localized protein that regulates autophagy and ER stress. *PLoS One* **8,** e64228 (2013).
23. Yompakdee, C., Ogawa, N., Harashima, S. & Oshima, Y. A putative membrane protein, Pho88p, involved in inorganic phosphate transport in *Saccharomyces cerevisiae*. *Mol. Gen. Genet.* **251,** 580–590 (1996).
24. Kulak, N. A., Pichler, G., Paron, I., Nagaraj, N. & Mann, M. Minimal, encapsulated proteomic-sample processing applied to copy-number estimation in eukaryotic cells. *Nat. Methods* **11,** 319–324 (2014).
25. Jan, C. H., Williams, C. C. & Weissman, J. S. Principles of ER cotranslational translocation revealed by proximity-specific ribosome profiling. *Science* **80,** 1257521 (2014). doi:10.1126/science.1257521
26. Noriega, T. R. *et al.* Signal recognition particle-ribosome binding is sensitive to nascent chain length. *J. Biol. Chem.* **289,** 19294–19305 (2014).
27. Pan, X. *et al.* A DNA integrity network in the yeast *Saccharomyces cerevisiae*. *Cell* **124,** 1069–1081 (2006).

Supplementary Information is available in the online version of the paper.

Acknowledgements We thank Schuldiner laboratory members for discussions and comments on the manuscript; D. Kaganovich, T. Ravid, J. Gerst, S. High and H. Riezman for plasmids; P. Walter and M. Seedorf for antibodies; and I. Yofe and U. Weill for the N-terminal tagging plasmid and primers. T.A. was supported by the Adams Fellowship Program of the Israel Academy of Sciences and Humanities. The work on human cells was supported by a DFG grant (IRTG 1830 and ZI 234/13-1) to R.Z. and the generation of anti-hSnd2 antibodies was funded by HOMFOR (HOMFOR2015). Supercomplex analysis by E.C.A. and B.S. was funded by the Deutsche Forschungsgemeinschaft (SFB 1190 P04). J.S.W. is supported by the NIH/NGMS (Center for RNA Systems Biology P50 GM102706 (Cate)). E.A.C. is supported by the National Science Foundation under grant 1144247. This work was funded by the Minerva foundation and Israel Science Foundation grant number 791/14 support to M.S. M.S is an incumbent of the Dr. Gilbert Omenn and Martha Darling Professorial Chair in Molecular Genetics.

Author Contributions N.A., T.A. and M.S. conceptualized the study; S.G.C., E.A.C and C.H.J. performed computational analysis; E.A.C. performed the ribosome profiling experiments, E.C.A. performed the blue-native page experiments; S.H., J.D., M.J. and S.S. performed the mammalian experiments; N.A. and T.A. performed all other experiments; T.A., B.S., R.Z., J.S.W. and M.S. supervised the study; N.A. and M.S. wrote the manuscript. All authors discussed the results and commented on the manuscript.

Author Information Reprints and permissions information is available at www.nature.com/reprints. The authors declare no competing financial interests. Readers are welcome to comment on the online version of the paper. Correspondence and requests for materials should be addressed to M.S. (maya.schuldiner@weizmann.ac.il) or T.A. (tast@broadinstitute.org).

METHODS

No statistical methods were used to predetermine sample size. The experiments were not randomized and the investigators were not blinded to allocation during experiments and outcome assessment.

Yeast strains and strain construction. Yeast strains are all based on the BY4741 laboratory strain[28]. Manipulations were performed using a standard PEG/LiAC transformation protocol[29]. All deletions were verified using primers from within the endogenous open reading frame. Primers for all genetic manipulations were planned either manually or using the Primers-4-Yeast web tool[30]. All strains, primers and plasmids used in this study[28,31–34] are listed in Supplementary Table 4.

Automated yeast library manipulations and high-throughput microscopy. SGA and microscopic screening were performed using an automated microscopy set-up as previously described[11,15], using the RoToR bench-top colony arrayer (Singer Instruments) and automated inverted fluorescent microscopic ScanR system (Olympus). Images were acquired using a 60× air lens with excitation at 490/20 nm and emission at 535/50 nm (GFP) or excitation at 575/35 nm and emission at 632/60 nm (RFP). After acquisition, images were manually reviewed using the ScanR analysis program.

Manual microscopy. Manual microscopy was performed using by one of two apparatuses. (I) Olympus IX71 microscope controlled by the Delta Vision SoftWoRx 3.5.1 software. Images were acquired using a 60× oil lens and captured by PhoetometricsCoolsnap HQ camera with excitation at 490/20 nm and emission at 528/38 nm (GFP/YFP) or excitation at 555/28 nm and emission at 617/73 nm (mCherry/RFP). (II) VisiScope Confocal Cell Explorer system, composed of a Zeiss Yokogawa spinning disk scanning unit (CSU-W1) coupled with an inverted Olympus IX83 microscope. Images were acquired using a 60× oil lens and captured by a connected PCO-Edge sCMOS camera, controlled by VisView software, with wavelength of 488 nm (GFP) or 561 nm (mCherry/RFP). Images were transferred to Adobe Photoshop CS6 for slight adjustments to contrast and brightness.

Co-immunoprecipitation. Lysates for immunoprecipitation were prepared from indicated strains in mid-logarithmic growth grown in YPD reach medium. Cells were harvested, washed in distilled water, and resuspended in lysis buffer (50 mM Tris HCl pH 7, 150 mM NaCl) supplemented with protease inhibitors (complete EDTA-free cocktail; Roche) and frozen in a drop-by-drop fashion in liquid nitrogen. Frozen cells were then pulverized in a ball mill (1 min at 30 Hz; Retsch) and thawed with nutation. Samples were thawed in 1 ml lysis buffer supplemented with protease inhibitors and 1% CHAPS (Sigma Aldrich) at 4 °C for 1 h. All samples were then clarified by centrifugation at 14,000*g* at 4 °C for 15 min. The remaining supernatant was added to GFP-trap (Chromotek) for 1 h followed by centrifugation at 1,000*g* at 4 °C for 3 min, and the supernatant was set aside as the flow through. Beads were washed three times with lysis buffer supplemented with protease inhibitors, and bound proteins were released from the beads by a 5-min incubation at 95 °C in sample buffer. The total protein lysate, the flow through and the immunoprecipitation (IP) fraction were analysed by western blotting.

Western blot analysis. Yeast proteins were extracted by either NaOH or TCA protocol as previously described[9,35] and resolved on polyacrylamide gels, transferred to nitrocellulose membrane blots, and probed with primary rabbit/mouse antibodies against HA (BioLegend, 901502), GFP (Abcam ab290), RFP (Abcam ab62341), histone H3 (Abcam ab1791), actin (Abcam ab8224), Sec65 (kindly provided by P. Walter) or Sec61 (kindly provided by M. Seedorf). The membranes were then probed with a secondary goat-anti-rabbit/mouse antibody conjugated to IRDye800 or to IRDye680 (LI-COR Biosciences). Membranes were scanned for infrared signal using the Odyssey Imaging System. Images were transferred to Adobe Photoshop CS6 for slight adjustments to contrast and brightness.

Metabolic labelling. Newly synthesized yeast proteins were radioactively labelled *in vivo* by a 7–10 min pulse with [^{35}S]methionine at either 30 °C or 37 °C. Labelling was stopped by adding to the cells ice-cold TCA to a final concentration of 10%. Cells were then lysed and proteins were immunoprecipitated as previously described[36] with antibodies against RFP (Abcam, ab62341), HA (BioLegend, 901502), Kar2 (kindly provided by P. Walter) or CPY (Abcam, ab113685). Protease inhibitors (complete EDTA-free cocktail; Roche) were used throughout the extraction and immunoprecipitation process. Immunoprecipitated samples were resolved on polyacrylamide gels, which were then exposed to Phosphor Screen (GE Life Sciences) and scanned by phosphorimager. Translocation efficiency was calculated as $\left[\left(\frac{\text{ER form}}{\text{total protein}}\right)_{\text{mutant}} / \left(\frac{\text{ER form}}{\text{total protein}}\right)_{\text{WT}}\right]$. The statistical significance of differences was measured using two-tailed student *t*-test with unequal variance, as indicated in the figure legends. For the Tetp-repression experiments, doxycycline (Sigma-Aldrich) was added to the overnight culture and to the back-dilution medium at a final concentration of 15 μg/ml.

Proximity-specific ribosome profiling. The ribosomal subunits RPL16a/b were conjugated to AVI-tag (biotin acceptor peptide), and Sec63 was conjugated to BirA (biotin ligase), allowing the specific biotinylation and streptavidin pull-down of ribosomes in close physical proximity to the ER membrane. By comparing the ribosomal footprints obtained from the total ribosome fraction and the streptavidin-pulled fraction, we measured ER-localized translation enrichment. Biotin induction was carried out at mid-logarithmic growth phase in the presence of cycloheximide, which was added to the medium 2 min before the addition of biotin, at a final concentration of 100 μg/ml. To induce biotinylation, D-biotin was added to the medium to a final concentration of 10 nM and biotinylation was allowed to proceed for 2 min at the same temperature as growth. Cells were harvested by filtration onto 0.45 μm pore size nitrocellulose filters (Whatman), scraped from the membrane, and immediately submerged in liquid nitrogen. The following steps of monosome isolation, streptavidin pulldown of biotinylated ribosomes, and library generation were done as previously described[25].

Ribosome profiling computational analysis. *Footprint sequence.* Sequencing reads were demultiplexed and stripped of 3′ cloning adapters using in-house scripts. Reads were mapped sequentially to Bowtie indices composed of rRNAs, tRNAs, and finally all chromosomes using Bowtie 1.1.0. Only uniquely-mapped, zero-mismatch reads from the final genomic alignment were used for subsequent analyses. These alignments were assigned a specific P-site nucleotide using a 15-nt offset from the 3′ end of reads.

Gene enrichments. Gene-level enrichments were computed by taking the $\log_2$ ratio of biotinylated footprint density (reads per million) within a gene coding sequence (CDS) over the corresponding density of matched input ribosome-profiling experiment. Yeast genes were excluded from all analysis if they met any of the following criteria: had fewer than 100 CDS-mapping footprints in the input sample of a particular experiment; were annotated as 'dubious' in the SGD database; mapped to the mitochondrial chromosome. Additionally, regions in which a CDS overlapped another same-strand CDS were excluded from enrichment calculations.

TMD classifications. TMD positions were predicted using the Phobius algorithm. TMD classification was divided based on the start site of the first predicted TMD: N-terminal TMDs start in the first 95 amino acids of the protein; downstream TMDs start after the first 95 amino acids of the protein.

SND-dependent genes. Genes that were dependent on SND components were identified by comparing the Sec63-BirA ER enrichment in a wild-type strain (yJW1784) with that in a *Δsnd* strain (yJW1811, yJW1812, or yJW1813) as previously described[25]. Briefly, $\log_2$ enrichments were separately normalized by subtracting the mean enrichment and dividing by the standard deviation of enrichments for the corresponding experiment. Genes were then binned by the minimum number of sequencing counts in either wild-type or *Δsnd* input sample, and the difference between normalized enrichments was compared within each bin. Enriched genes were defined as those genes whose *Δsnd* $\log_2$ enrichments were greater than 0.3 and whose enrichments increased in the *Δsnd* sample by at least two standard deviations compared to other genes in that bin. Depleted genes were defined as those genes whose wild type $\log_2$ enrichments were greater than 0.3 and whose enrichments decreased in the *Δsnd* sample by at least two standard deviations compared to other genes in that bin. Significant depletion of 10–23%, 9–42% and 14–45% was observed in *Δsnd1*, *Δsnd2* and *Δsnd3*, respectively. Including or excluding SS-bearing proteins had no effect on this trend. Mitochondrial proteins were excluded from the analysis.

Immunoprecipitation followed by mass spectrometry. Lysates for immunoprecipitations were prepared from yeast that expressed GFP-tagged SND genes or a constitutively expressed GFP-negative control, in mid-logarithmic growth grown in YPD reach medium. Cells were harvested, washed in distilled water, and resuspended in lysis buffer (50 mM Tris HCl pH 7, 150 mM NaCl) supplemented with protease inhibitors (complete EDTA-free cocktail; Roche) and frozen in a drop-by-drop fashion in liquid nitrogen. Frozen cells were then pulverized in a ball mill (1 min at 30 Hz; Retsch) and thawed with nutation. Samples were thawed in 1 ml lysis buffer supplemented with protease inhibitors and 1% digitonin (Sigma Aldrich) at 4 °C for 1 h. All samples were then clarified by centrifugation at 14,000*g* at 4 °C for 15 min. The remaining supernatant was added to GFP-trap (Chromotek) for 1 h followed by three washes with lysis buffer supplemented with protease inhibitors and 1% digitonin. Bound proteins were released from the beads by a 5-min acidic treatment (0.2 M glycine pH 2.5), which was neutralized with 1 M Tris pH 9.4. The eluted proteins were digested with 0.4 μg sequencing grade trypsin for 2 h in the presence of 100 μl of 2 M urea, 50 mM Tris HCl pH 7.5 and 1 mM DTT. The resulting peptides were acidified with trifluoroacetic acid (TFA) and purified on C18 StageTips. LC–MS/MS analysis was performed on an EASY-nLC1000 UHPLC (Thermo Scientific) coupled to a Q-Exactive mass spectrometer (Thermo Scientific). Peptides were loaded onto the column with buffer A (0.5% acetic acid) and separated on a 50-cm PepMap column (75 μm i.d., 2 μm beads; Dionex) using a 4-h gradient of 5–30% buffer B (80% acetonitrile, 0.5% acetic acid). Interactors were extracted by comparing the protein intensities to a GFP control.

Blue native gel electrophoresis. Yeast microsomes were extracted from the ADHp-SND2–GFP/SND3–HA strain as described[37]. In brief, spheroplasts of yeast were lysed by dounce homogenization (25 strokes) in lysis buffer (0.1 M sorbitol, 20 mM HEPES pH 7.4, 50 mM potassium acetate, 2 mM EDTA, 1 mM DTT, 1 mM PMSF) at 4 °C. The lysates were centrifuged at 1,000*g* and the resulting supernatant at 27,000*g* for 10 min at 4 °C. The crude membrane pellet was re-suspended in lysis buffer and layered onto a discontinuous sucrose density gradient consisting of 1.2 and 1.5 M sucrose. Following centrifugation at 100,000*g* for 60 min at 4 °C, the membranes at the 1.2–1.5 M sucrose interface were collected and washed twice in lysis buffer. The membrane pellets were re-suspended in membrane storage buffer (50 mM NaCl, 0.32 M sucrose, 20 mM HEPES pH 7.4, 2 mM EDTA containing protease inhibitors) and the protein concentration determined by a standard Bradford assay.

Microsomes were solubilized in ComplexioLyte 48 buffer (1 mg/ml, Logopharm) for 30 min at 4 °C[38]. Solubilized extracts were centrifuged at 100,000*g* for 30 min at 4 °C, supplemented with glycerol (5%) and coomassie G-250 (0.3%) and loaded on a 3.5–15% linear native polyacrylamide gel. The BN-PAGE gel was prepared as described[39]. The gel buffer contained 25 mM imidazole and 500 mM 6-aminohexanoic acid. The cathode chamber was first filled with cathode buffer B (50 mM Tricine, 7.5 mM imidazole and 0.02% coomassie) and subsequently replaced by cathode buffer B/10 (containing 0.002% coomassie) after the gel running front had covered a third of the desired distance of electrophoresis. The anode chamber was filled with 25 mM imidazole pH 7.0. A high-molecular-weight calibration kit for native electrophoresis from GE Healthcare was used as a standard. For 2D BN-PAGE, the excised lanes were equilibrated in 2D-dissociation buffer (60 mM Tris/HCl pH 6.8, 10% glycerol, 2% SDS, 5% v/v β-mercaptoethanol, 6 M urea) before separation on the second dimension by SDS–PAGE. After electro-blotting, the nitrocellulose membrane was detected with the indicated antibodies.

Analysis of human cells. The HEK293 cell line used was obtained from DSMZ (no. ACC 305). DSMZ supplied verification of authentication of the cells, tested by DSMZ via short tandem repeat loci (STR profile). The cell line is routinely tested for mycoplasma contamination. This cell line was chosen as it is routinely used for fractionation experiments.

Rough microsomes from human cells were prepared as described[40]. Briefly, 30×10^6 HEK293 cells were harvested and washed once with PBS and twice with buffer 1 (50 mM HEPES/KOH pH 7.5; 0.25 M sucrose; 50 mM KOAc; 6 mM MgOAc; 4 mM PMSF; 1 mM EDTA; 1 mM DTT; 0.1 mg/ml cycloheximide; 0.3 U/ml RNAsin (Promega); protease inhibitor cocktail). After homogenization in buffer 1 using a glass/Teflon homogenizer, the suspension was centrifuged at 1,000*g* for 10 min. The supernatant was centrifuged at 10,000*g* for 10 min. The new supernatant was layered onto 0.6 M sucrose in buffer 2 (50 mM HEPES/KOH pH 7.5, 0.6 M sucrose, 100 mM KOAc, 5 mM MgOAc, 4 mM DTT, 0.1 mg/ml cycloheximide, 40 U/ml RNAsin) and centrifuged at 230,000*g* for 90 min. The resulting membrane pellet was previously shown to comprise rough ER. Here, it was resuspended in buffer 2 and adjusted to 2.3 M sucrose, which was overlaid with 1.9 and 0 M sucrose, respectively, in buffer 2. After flotation at 100,000*g* for 18 h, the interphase between 0 and 1.9 M sucrose, two fractions of the remaining supernatant, and the pellet were collected. After centrifugation of the interphase at 100,000*g* for 1 h, the membrane pellet corresponded to purified rough ER. All steps after the first washing step were carried out on ice.

Western blot analyses employed antibodies against β-actin (Sigma), CAML (Synaptic Systems SA7679), or rabbit antibodies that were raised against the depicted proteins: the C-terminal peptide of hSnd2 (KRQRRQERRQMKRL) plus an N-terminal cysteine; or an internal peptide of SRα (KKFEDSEKAKKPVR) plus a C-terminal cysteine, cross-linked to KLH. The SRα and β-actin antibodies were visualized using ECL Plex goat-anti-rabbit IgG-Cy5-conjugate or ECL Plex goat-anti-mouse IgG-Cy3-conjugate (GE Healthcare) and the Typhoon-Trio imaging system (GE Healthcare) in combination with Image Quant TL software 7.0 (GE Healthcare). The hSnd2 and CAML antibodies were visualized using secondary peroxidase (POD)-coupled anti-rabbit antibody (Sigma) plus ECL (GE Healthcare) and the Fusion SL luminescence-imaging system (Peqlab) in combination with Image Quant TL software 7.0.

Data availability. Ribosome-profiling data have been deposited in Gene Expression Omnibus (GEO) under accession number GSE85686. Gel source images can be found in Supplementary Fig. 1. Other data that support the findings of this study are available from the authors on reasonable request.

28. Brachmann, C. B. *et al.* Designer deletion strains derived from *Saccharomyces cerevisiae* S288C: a useful set of strains and plasmids for PCR-mediated gene disruption and other applications. *Yeast* **14,** 115–132 (1998).
29. Gietz, R. D. & Woods, R. A. Transformation of yeast by lithium acetate/single-stranded carrier DNA/polyethylene glycol method. *Methods Enzymol.* **350,** 87–96 (2002).
30. Yofe, I. & Schuldiner, M. Primers-4-Yeast: a comprehensive web tool for planning primers for *Saccharomyces cerevisiae*. *Yeast* **31,** 77–80 (2014).
31. Longtine, M. S. *et al.* Additional modules for versatile and economical PCR-based gene deletion and modification in *Saccharomyces cerevisiae*. *Yeast* **14,** 953–961 (1998).
32. Kitada, K., Yamaguchi, E. & Arisawa, M. Cloning of the *Candida glabrata TRP1* and *HIS3* genes, and construction of their disruptant strains by sequential integrative transformation. *Gene* **165,** 203–206 (1995).
33. Goldstein, A. L. & McCusker, J. H. Three new dominant drug resistance cassettes for gene disruption in *Saccharomyces cerevisiae*. *Yeast* **15,** 1541–1553 (1999).
34. Stirling, C. J. & Hewitt, E. W. The *S. cerevisiae SEC65* gene encodes a component of yeast signal recognition particle with homology to human SRP19. *Nature* **356,** 534–537 (1992).
35. Kushnirov, V. V. Rapid and reliable protein extraction from yeast. *Yeast* **16,** 857–860 (2000).
36. Graham, T. R. Metabolic labeling and immunoprecipitation of yeast proteins. *Curr. Protoc. Cell Biol.* **7,** 7.6 (2001).
37. Wuestehube, L. J. & Schekman, R. W. Reconstitution of transport from endoplasmic reticulum to Golgi complex using endoplasmic reticulum-enriched membrane fraction from yeast. *Methods Enzymol.* **219,** 124–136 (1992).
38. Schwenk, J. *et al.* Functional proteomics identify cornichon proteins as auxiliary subunits of AMPA receptors. *Science* **323,** 1313–1319 (2009).
39. Wittig, I., Braun, H.-P. & Schägger, H. Blue native PAGE. *Nat. Protocols* **1,** 418–428 (2006).
40. Pfeffer, S. *et al.* Structure of the mammalian oligosaccharyl-transferase complex in the native ER protein translocon. *Nat. Commun.* **5,** 3072 (2014).

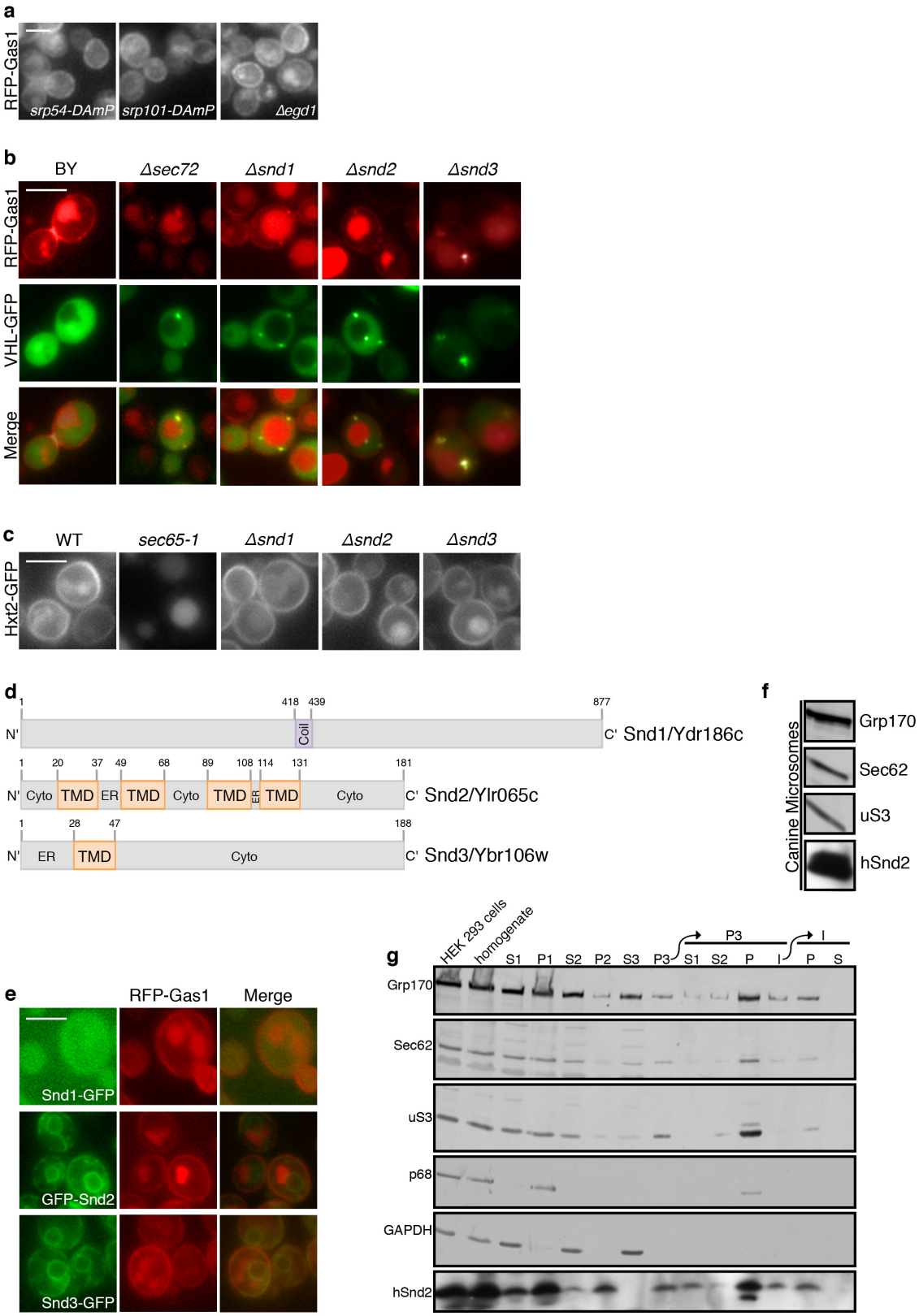

Extended Data Figure 1 | See next page for caption.

Extended Data Figure 1 | The SND proteins mediate SRP-independent targeting. a, Fluorescent micrographs of RFP–Gas1 confirm that it is not mislocalized when components of SRP, SRP receptor or NAC are compromised (control image can be found in Fig. 1b). Scale bars throughout figure, 5 μm. Images throughout figure are representative of about 300 cells captured per strain. **b**, *SND* mutants accumulate RFP–Gas1 in inclusions. Fluorescent micrographs confirm that accumulations of RFP–Gas1 in *Δsnd* strains colocalize with the cytosolic inclusion marker VHL–GFP. **c**, *SND* deletions do not have a non-specific effect on translation, targeting or translocation. A fluorescently tagged SRP substrate (Hxt2–GFP) was mislocalized only in the temperature-sensitive strain *sec65-1* when grown at the restrictive temperature of 37 °C (under these conditions the cells lack functional SRP). *SND*-deleted strains display normal cell surface localization of Hxt2. **d**, Schematic representation of the structural elements and topology predictions of Snd1 (top), Snd2 (middle) and Snd3 (bottom). Numbers indicate the number of amino acids in the proteins. **e**, RFP–Gas1 is correctly localized in all GFP-tagged SND proteins, indicating that the tag does not disrupt their function and endogenous localization. **f**, A mammalian orthologue of Snd2 (hSnd2) is present in canine pancreatic rough microsomes, which are routinely used as a source of mammalian ER proteins, as seen by immunoblotting with an antibody (data not shown) against hSnd2 that was shown to be specific by siRNA-mediated gene silencing. **g**, Endogenous hSnd2 is localized to human rough ER. HEK293 cells were homogenized and subfractionated into various pellet (P) and supernatant (S) fractions. Fractions were analysed by SDS–PAGE and immunoblotting. hSnd2 co-fractionated with the rough ER markers Grp170 and Sec62 and the ribosomal protein uS3 but not with the nuclear and cytosolic proteins p68 and GAPDH. The areas of interest of luminescence images from a single western blot are shown. For gel source images see Supplementary Fig. 1.

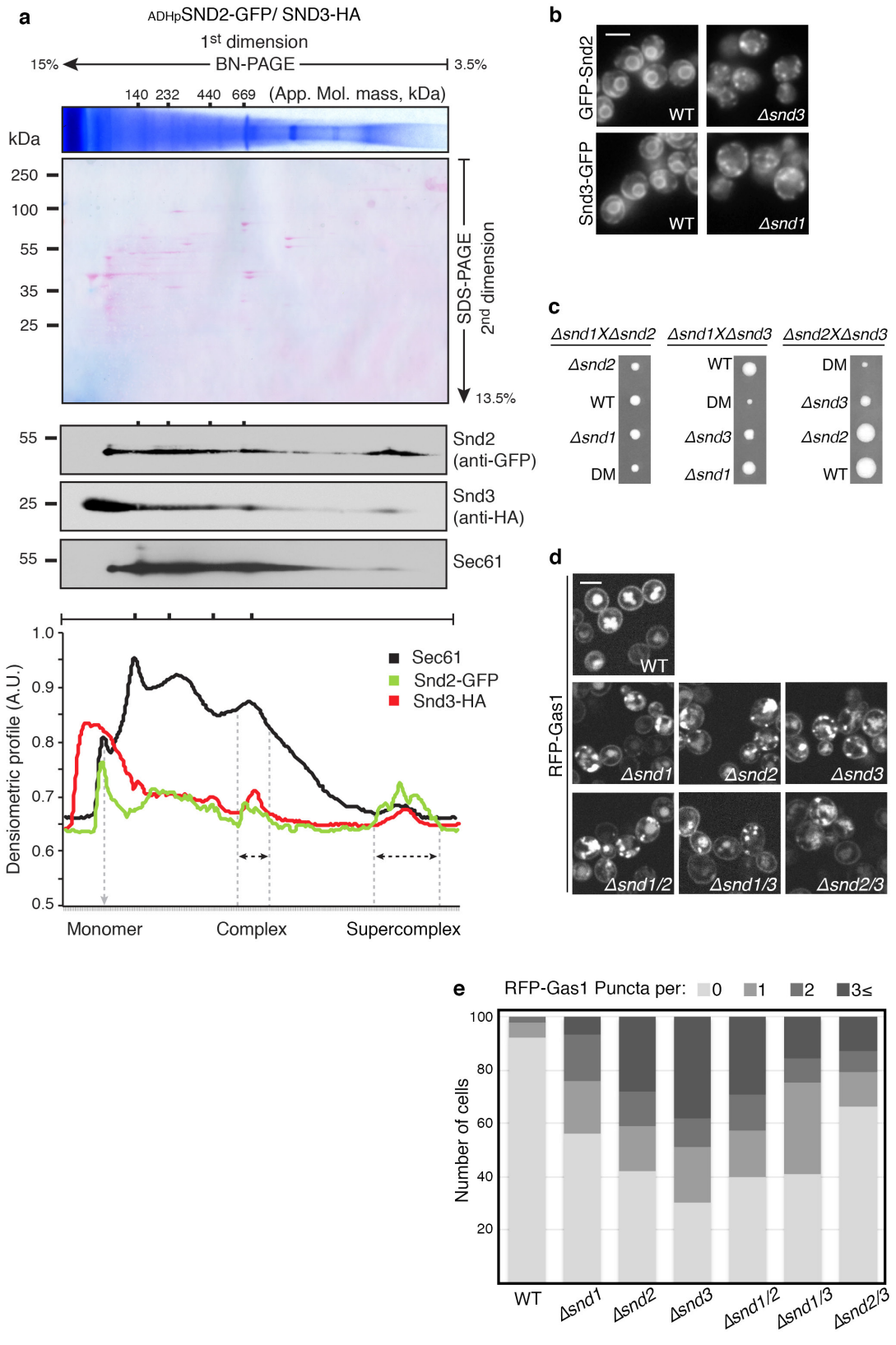

Extended Data Figure 2 | See next page for caption.

Extended Data Figure 2 | The SND proteins function in a joint targeting pathway. a, Snd2 and Snd3 form a complex with the Sec61 translocon, as shown by BN-PAGE followed by second-dimension SDS–PAGE. Densitometry quantification revealed that Sec61 migrates in four distinct complexes as well as a monomer. Snd2 and Snd3 reside together in two of these complexes, one approximately 669 kDa and a second with a higher molecular mass. We postulate that the two Sec61–SND complexes may differ in size depending on the presence of additional auxiliary components. For gel source images see Supplementary Fig. 1. **b**, Fluorescent micrographs showing that Snd2 is mislocalized upon deletion of *SND3* and Snd3 is mislocalized upon deletion of *SND1*, suggesting functional dependence among the three proteins. Scale bars throughout figure, 5 μm. Images throughout figure are representative of around 300 cells captured per strain. **c**, Growth rates reveal genetic interactions among the *SND* genes. Heterozygous diploids of *Δsnd* were sporulated and tetrad-dissected to retrieve haploids. Tetrads obtained demonstrate an epistatic interaction between *SND1* and *SND2* mutations, and a synthetic sick interaction between *SND3* and the *SND1/2* mutations. As *SND3* is more than an order of magnitude more abundant than *SND1/2*, it is possible that this interaction is due to an independent cellular function. **d**, Fluorescent micrographs of RFP–Gas1 in single and double *SND* mutants show that the mutations are epistatic to each other in terms of their effect on targeting. **e**, Quantification of the RFP–Gas1 mislocalization phenotype in *SND* single and double mutants (Extended Data Fig. 2d) reveals a buffering epistatic interaction between *SND* genes (100 cells were counted per strain).

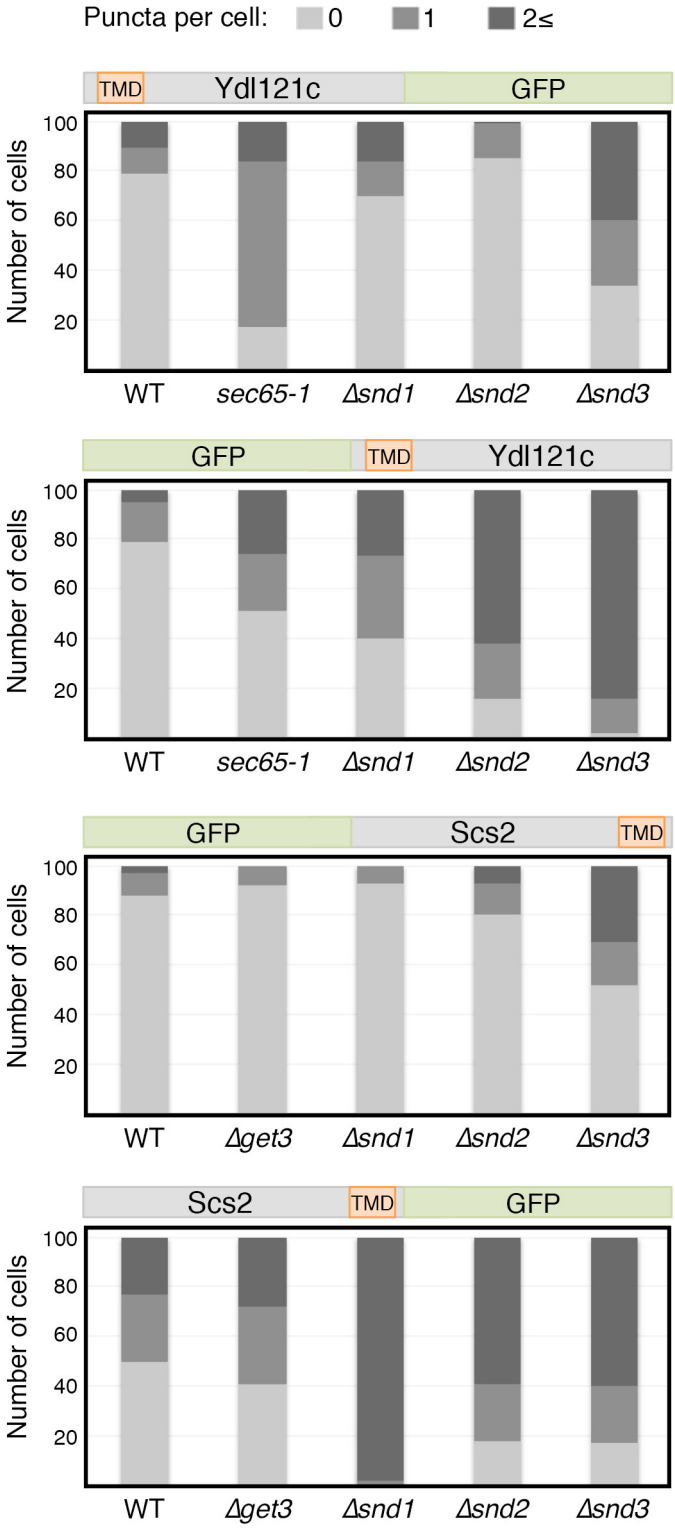

Extended Data Figure 3 | Substrate affinity to a targeting pathway depends on the position of its transmembrane domain. Quantification of the mislocalization phenotype in Fig. 2f, g confirms that re-positioning of a substrate's TMD can alter its dependence on the different targeting pathways.

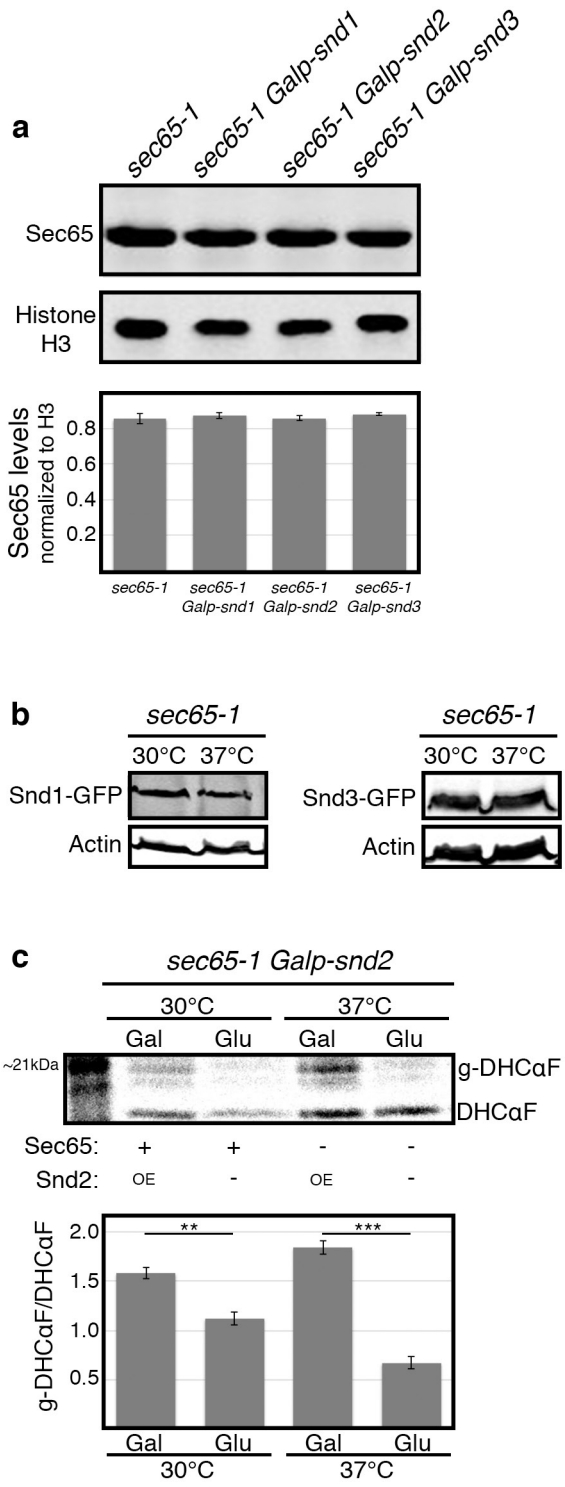

Extended Data Figure 4 | Compensation for loss of SRP by the SNDs is not due to alteration in protein levels. a, Overexpression of *SND* genes does not affect SRP levels. *SND* genes were overexpressed by growth on galactose in 30 °C, and levels of Sec65 protein were measured by western blotting and normalized to a histone H3 loading control. No apparent change in *sec65-1* levels was detected, implying that the rescue observed in Fig. 3b–d is not due to increased SRP levels (data shown as mean ± s.e.m., $n = 3$, no statistically significant difference was seen between the samples, biological replicates). **b**, Levels of SND proteins do not change in SRP-depleted cells. SND proteins were C-terminally tagged on the *sec65-1* background, and their levels were measured by western blotting when grown at either permissive or restrictive temperatures (30 °C and 37 °C, respectively), and normalized to an actin loading control. No apparent change in Snd1 or Snd3 levels was observed. Snd2 levels were below detection threshold (data not shown). **c**, Pulse radioactive metabolic labelling followed by DHCαF immunoprecipitation was used to measure the translocation rate of DHCαF. *SND2* overexpression induced significantly higher translocation when compared to its repression by glucose, regardless of the functional state of *sec65-1*. Data shown as mean ± s.e.m. $^{**}P < 0.01$, $^{***}P < 0.001$, by two-tailed Student's *t*-test, $n = 3$, biological replicates. For all gel source images see Supplementary Fig. 1.

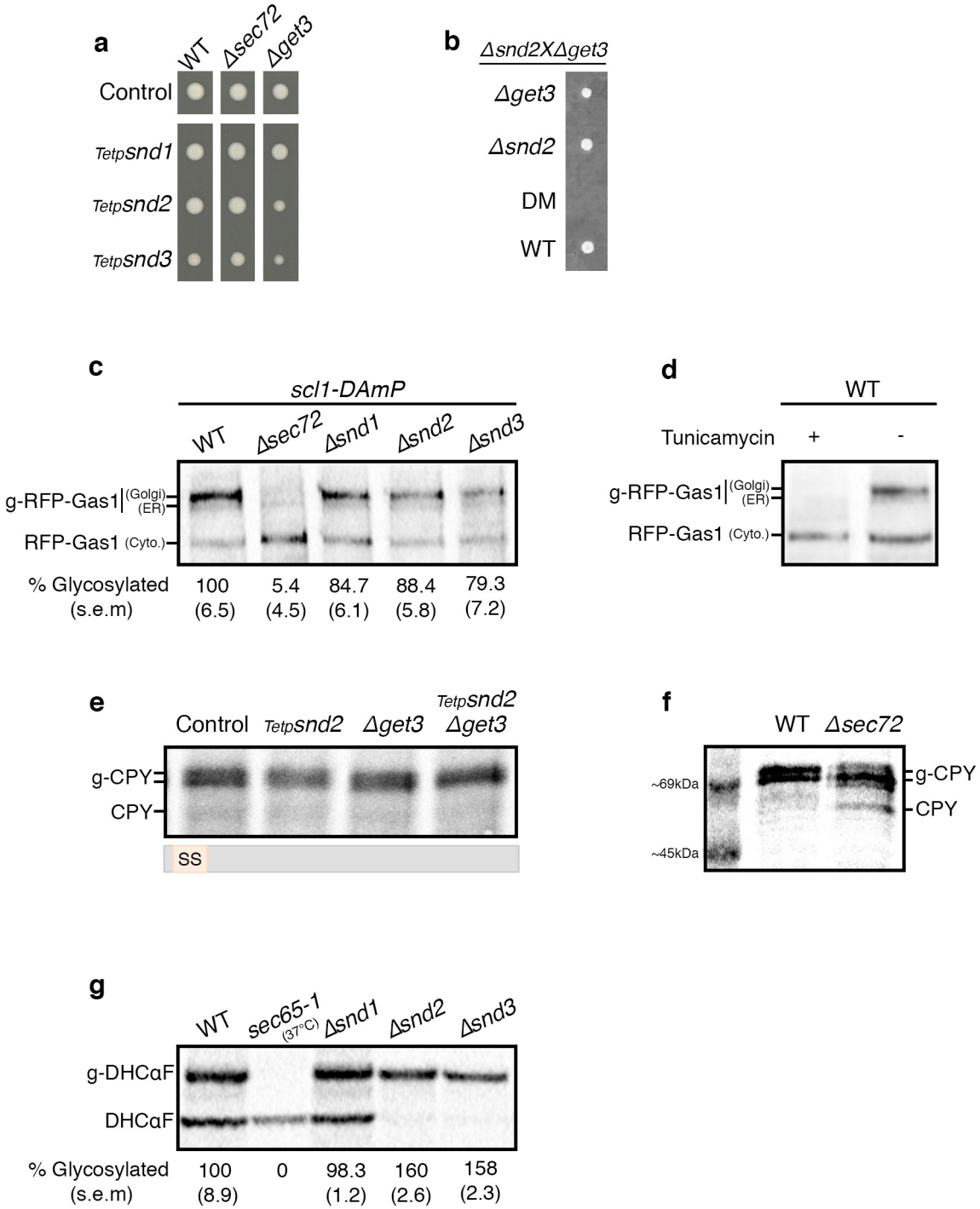

Extended Data Figure 5 | See next page for caption.

Extended Data Figure 5 | The GET and SND pathways are partially redundant. a, Repression of *SND* genes is epistatic with *SEC72* deletion and synthetic sick with *GET3* deletion. Growth rates of strains with the *SND* genes expressed under the regulation of a repressible Tet-promoter when grown on tetracycline. The growth rate of *Δsec72 Tetp-SNDs* conditional double mutants is identical to that of the control strain, indicating that these mutations are epistatic. The *Δget3 Tetp-SNDs* conditional double mutants are sick, but viable. **b**, Double deletion of *SND2* and *GET3* is lethal. Heterozygous diploids of *Δsnd2* and *Δget3* were sporulated and tetrad-dissected to retrieve haploids. Tetrads obtained demonstrate a synthetic lethal interaction between *SND2* and *GET3*. **c**, RFP–Gas1 translocation is moderately affected by *SND* single deletions. Pulse radioactive metabolic labelling followed by RFP–Gas1 immunoprecipitation was used to measure RFP–Gas1 translocation rates. Percentage of glycosylated ER and Golgi forms (indicated by two black lines) was reduced to 5% in *Δsec72* mutants, while in *Δsnd1*, *Δsnd2* and *Δsnd3* strains it was reduced to 85%, 88% and 79%, respectively (data shown as mean (s.e.m.), $n = 3$, biological replicates). All strains in this assay were attenuated for degradation with the *scl1-DAmP* proteasome hypomorphic allele. **d**, Pulse radioactive metabolic labelling followed by RFP–Gas1 immunoprecipitation was performed in the presence and absence of the glycosylation inhibitor tunicamycin, allowing the identification of three forms of RFP–Gas1: cytosolic, ER and Golgi (mature). **e**, CPY targeting is not affected by double mutants of the SND and GET pathways. The same methodology as in **c** was used to follow the signal sequence (SS)-containing protein CPY in the conditional *SND2/GET3* double mutant. A mild decrease in the glycosylated forms was observed in the *SND2* single mutant, but there was no translocation defect in the *GET3* single mutant or in the conditional double mutant. This result was repeated in three independent biological replicates. **f**, CPY was metabolically labelled in a control strain and a partially translocated pool was visualized with a ladder to provide a size reference to **e**. **g**, The same methodology as in **c** was used to measure the translocation rate of the SRP-dependent substrate DHCαF. In the temperature-sensitive strain *sec65-1*, at the restrictive temperature (37 °C), there was no translocated substrate. The translocation efficiency of the *Δsnd1* strain was comparable to that of the wild-type control; in the *Δsnd2* and *Δsnd3* strains it was significantly higher (~160% glycosylated protein compared to the wild-type control). Data shown as mean (s.e.m.), $n = 3$, biological replicates. For all gel source images see Supplementary Fig. 1.